Atmos. Meas. Tech. Discuss., doi:10.5194/amt-2016-362, 2016
Manuscript under review for journal Atmos. Meas. Tech.
Published: 25 November 2016

Atmospheric Measurement Techniques Discussions

Airborne remote sensing and in-situ measurements of atmospheric CO_2 to quantify point source emissions

Thomas Krings[1], Bruno Neininger[2], Konstantin Gerilowski[1], Sven Krautwurst[1], Michael Buchwitz[1], John P. Burrows[1], Carsten Lindemann[3], Thomas Ruhtz[3], Dirk Schüttemeyer[4], and Heinrich Bovensmann[1]

[1]Institute of Environmental Physics, University of Bremen, FB 1, P.O. Box 330440, D-28334 Bremen, Germany
[2]METAIR AG, Airfield Hausen am Albis, CH-8915 Hausen am Albis, Switzerland
[3]Institute for Space Sciences, Free University of Berlin, Carl-Heinrich-Becker-Weg 6-10, D-12165 Berlin, Germany
[4]ESA / ESTEC, Keplerlaan 1, 2201 AZ Noordwijk, The Netherlands

Correspondence to: Thomas Krings (Thomas.Krings@iup.physik.uni-bremen.de)

Abstract. Reliable techniques to infer greenhouse gas emission rates from localised sources require accurate measurement and inversion approaches. In this study airborne remote sensing observations by the MAMAP instrument and airborne in-situ measurements are used to infer emission estimates of carbon dioxide released from a cluster of coal fired power plants. For the analysis of in-situ data, a mass balance approach is described and applied. Whereas for the remote sensing observations an inverse Gaussian plume model is used in addition to a mass balance technique. A comparison between methods shows that results for all methods agree within a few percent for cases where in-situ measurements were made for the complete vertical plume extent. Even though the power plants are partly in close proximity and the associated carbon dioxide plumes are overlapping it is possible to derive emission rates from remote sensing data for individual power plants that agree well with results derived from emission factors and energy production data for the time of the overflight.

1 Introduction

Knowledge of emissions of the greenhouse gases carbon dioxide (CO_2) and methane (CH_4) originating from localised sources is often inadequate (Ciais et al., 2015; NRC, 2010).

Even for well monitored localised CO_2 emitters, there are significant differences between inventories calculated using different but plausible methods. For example, Ackerman and Sundquist (2008) found differences of more than 20% between emissions from U.S. power plants. Differences in inventories of about a factor of two were found for CO_2 emissions from flaring in the oil and gas production (Ciais et al., 2015),

Similarly, the magnitude of fugitive emissions of natural gas, which comprises predominantly CH_4, is not clear and results from the lack of measurements (Kirschke et al., 2013; Howarth et al., 2012; Cathles et al., 2012; Allen et al., 2013). Recent studies using different methods show that there are significant disagreements between process based bottom up inventories on the one hand and top down emission estimates based on atmospheric measurements on the other hand (Karion et al., 2013; Schneising et al., 2014; U.S. Environmental Protection Agency, 2014). This is particularly relevant because losses of CH_4

Atmos. Meas. Tech. Discuss., doi:10.5194/amt-2016-362, 2016
Manuscript under review for journal Atmos. Meas. Tech.
Published: 25 November 2016

Atmospheric Measurement Techniques Discussions

from the use of natural gas from traditional sources or fracking negate the benefits in reducing global warming when using natural gas as an energy source in the transition from coal based to alternative renewable energy sources (Brandt et al., 2014; IPCC, 2006; Alvarez et al., 2012). These benefits result from its lower specific carbon dioxide emissions per Joule of energy compared to burning coal.

Top down estimates of localised sources are generally obtained using airborne or ground based in-situ measurements. Recently also the use of airborne remote sensing has demonstrated the ability to accurately estimate emissions. All methods have their distinctive advantages and disadvantages. Ground based in-situ measurements are fairly low-cost. However, they do generally not sample the complete atmospheric boundary layer, which is necessary for an accurate emission estimate. Airborne in-situ allows accurate concentration and wind speed measurements from which emissions can be derived (e.g. Karion et al., 2013; Caulton et al., 2014; Lavoie et al., 2015), but optimally require a vertically dense flight pattern. In addition assumptions about the lowest atmospheric layer have to be made that can usually not be accessed by aircraft. Furthermore air space restrictions can interfere with required flight patterns. Remote sensing allows sounding of the complete boundary layer and offers the opportunity to survey large areas in short time spans (Krings et al., 2011, 2013; Thompson et al., 2015; Frankenberg et al., 2016; Thorpe et al., 2014; Tratt et al., 2014). In contrast to in-situ measurements, however, clear sky conditions are mostly required except for those instruments operating in the thermal infrared (e.g. Tratt et al., 2014). Furthermore, wind information has to be additionally gathered for example from model data (see, for example, Krings et al., 2011) or additional in-situ wind measurements (see, for example, Krings et al., 2013).

Using the example of CO_2 emissions from a cluster of power plants in western Germany, top down results from airborne in-situ and remote sensing are evaluated and compared to each other, as well as to an independent bottom up estimate computed from energy production and emission factors. Additional complexity is added to the top down inverse problem since sources are partly located in close proximity to each other with overlapping CO_2 plumes. Generally, it is necessary to achieve a correct source attribution in the presence of multiple neighbouring sources for validation purposes. This provides insights into origin and specific processes that lead to the generation of greenhouse gases.

2 Measurement campaign and instrumentation

An airborne measurement campaign combining remote sensing measurements of XCO_2 and XCH_4 with in-situ measurements of atmospheric CO_2 and CH_4 concentration as well as wind speed and direction in the boundary layer took place in Germany in August 2012. This campaign was carried out in the framework of ESA's Earth Explorer 8 activities for the candidate mission CarbonSat (Bovensmann et al., 2010; Buchwitz et al., 2013).

For the remote sensing of the greenhouse gases CO_2 and CH_4, MAMAP was flown above the boundary layer on the Cessna T207A aircraft of the Free University of Berlin. MAMAP (Gerilowski et al., 2011) is an airborne 2 channel NIR-SWIR grating spectrometer system for accurate measurements of gradients in column-averaged methane and carbon dioxide concentrations. It was jointly developed by the Institute of Environmental Physics / Remote Sensing (IUP/IFE), University of Bremen (Germany) and the Helmholtz Centre Potsdam, German Research Centre for Geosciences (GFZ). It was demonstrated that the instrument

Atmos. Meas. Tech. Discuss., doi:10.5194/amt-2016-362, 2016
Manuscript under review for journal Atmos. Meas. Tech.
Published: 25 November 2016

Atmospheric Measurement Techniques Discussions

is able to detect and retrieve the total dry column of the greenhouse gases CH_4 and CO_2 with a precision of 0.3–0.4% ($1\,\sigma$) at local scales ($\approx$10 km), and that MAMAP is an appropriate tool for detection and inversion of localised greenhouse gas emissions from aircraft (Gerilowski et al., 2011; Krings et al., 2011, 2013).

For the in-situ airborne measurements, the small research aircraft METAIR TTC-ECO-DIMO was flown in the boundary layer to perform measurements in the plume emitted from the target, to perform background concentration measurements and to perform wind measurements needed for the interpretation of the total column measurements of MAMAP. The aircraft is equipped with underwing-pods, carrying up to 50 kg scientific payload each. The standard equipment measures the meteorological parameters wind (three-dimensional components in turbulent resolution), fast temperature and fast, redundant humidity. A two-channel aerosol counter (MetOne for >0.3 µm and >0.5 µm) can characterise the structure of the boundary layer. The chemical measurements are for CO_2 (redundant) and CH_4 corrected for H_2O interference (dilution and spectroscopic; details see Hiller et al. (2014)) as well as CO, O_3, NO_2, NO_x, NO_y, O_x. The methane monitor is a "Los Gatos DLT-100 Fast Methane Analyser" which was purchased by ETH Zurich and modified in a joint project. The CO_2 is measured with three different time resolutions and accuracies, resulting in an overall accuracy and precision of 0.4 ppm. The individual contributions are: (i) a fast (10 Hz) measurement with a short-term precision (e.g. while crossing a plume) of about 0.2 ppm, with a limited absolute accuracy of about 5 ppm, using a modified LiCor LI-7500. (ii) A more accurate continuous, but slower (0.3 Hz) reference with a modified LI-6262, with an accuracy of better than 0.5 ppm. The highest accuracy is from flask-samples (typically 9 per flight), analysed at MPI Jena. This method is described in Hiller et al. (2014).

The surveying strategy was to simultaneously probe the atmospheric boundary layer with in-situ measurements while the MAMAP remote sensing measurements were performed via the separate aircraft above.

3 Target area

While the complete campaign covered also other CO_2 and CH_4 emitting targets (Bovensmann et al., 2014) this study focuses on measurements obtained in an area with several lignite fired power plants in western Germany close to the city of Düsseldorf (see Fig. 1) on 15 August 2012. The power plants are Niederaußem, Neurath (old and new blocks) and Frimmersdorf. The remote sensing flights were performed at about 11:50 – 13:40 UTC (that is 13:50 – 15:40 local time, CEST). The in-situ survey over the same area was conducted between about 12:15 and 14:20 UTC. Wind was blowing approximately from South-East so that the CO_2 plumes of individual power plants were overlapping. Variation of the surface elevation in the immediate vicinity of the power plants was rather low in particular for the area in between power plants. The location of the open cast mines, visible as surface depressions, have shifted since the topography measurements shown in Fig. 1 as can be seen from more recent imagery available, for example, via GoogleEarth. The open cast mine west of Frimmersdorf has been moved further to the West, wheras that south of Niederaußem has been closed and refilled.

Atmos. Meas. Tech. Discuss., doi:10.5194/amt-2016-362, 2016
Manuscript under review for journal Atmos. Meas. Tech.
Published: 25 November 2016

Atmospheric Measurement Techniques Discussions

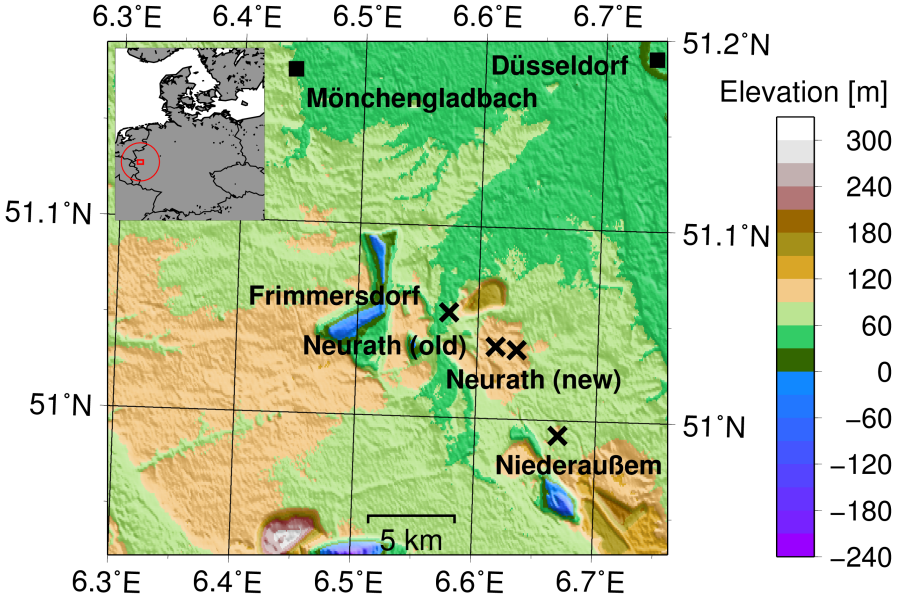

Figure 1. Map of the target area in western Germany. The crosses denote the four lignite fired power plants in the area. Topographic data have been obtained from the Shuttle Radar Topography Mission (SRTM) version 2.1 (http://dds.cr.usgs.gov/srtm/version2_1/), a collaborative effort from NASA, NGA as well as the German and Italian Space Agencies.

4 Methodology

4.1 Flux estimates from in-situ measurements

Calculating fluxes of trace gases through an imaginary vertical plane is trivial when the concentration field and the wind field are known for a sufficient time during quasi stationary conditions. However, in reality, such perfect measurements are not possible. Not the accuracy or precision of the measurements are a prime concern, but, unknown parts in the fields (inter- and extrapolations), and - most important - remaining instationarities both by short-term fluctuations (hitting a part of a plume or not), and by varying source strengths and changing meteorological conditions. Lavoie et al. (2015) and Caulton et al. (2014) discuss comparable airborne in-situ observations downwind of regions and individual sources. Their basic methods are described in Mays et al. (2009). The instrumentation and methods that were used in the work presented here are quite similar. However, by comparing the two approaches that were developed independently, three main differences can be identified: (i) The method of inter- and extrapolation of concentrations and winds are more transparent and straight forward here, where "Kriging" as applied in the referenced work is not necessarily best suitable for this type of data set. (ii) Here, also turbulent fluxes are included, both in the horizontal, and in the vertical. (iii) Due to a slower aircraft with an optimized wind measuring system, the accuracy of the wind field is slightly better. According to Mays et al. (2009), the measured wind vectors were of

Atmos. Meas. Tech. Discuss., doi:10.5194/amt-2016-362, 2016
Manuscript under review for journal Atmos. Meas. Tech.
Published: 25 November 2016

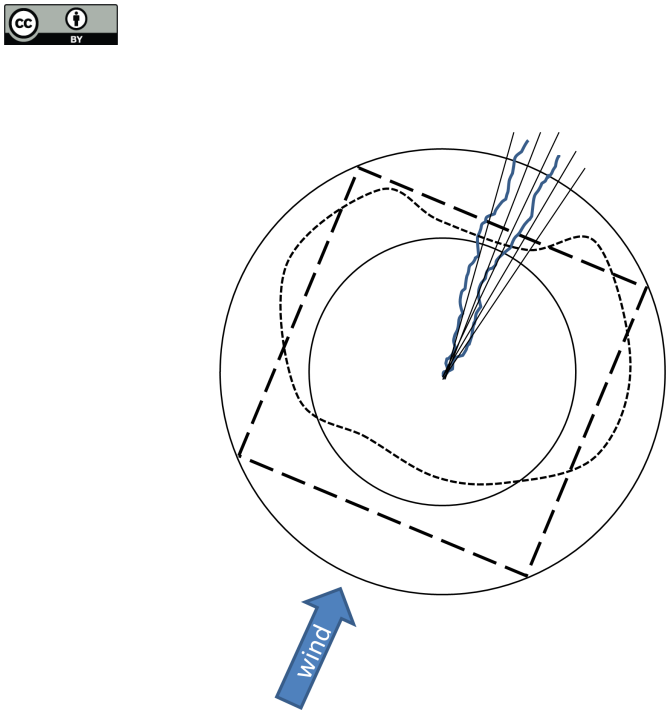

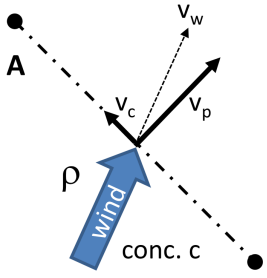

Figure 2. A two-dimensional area limited by two cylinders of different radius, by a rectangular box, or by an irregular boundary, with a plume leaving the area. In all these cases, the net flux out of the defined region is concentrated within the part of the boundary, where the plume is crossing. The radial lines along the plume are indicating that instead of the length of a boundary, also angles from a polar coordinate system could be used. The detail on the right is showing the incremental calculation of any fluxes through any shape of boundary: the flux is the product of area A, the density ρ, the concentration c, and the perpendicular wind component v_p, with the wind vector v_w, and the crosswind component v_c.

limited accuracy. It was decided to use modeled wind fields instead. In later work of this group (Lavoie et al., 2015), the wind measurements might have been improved. However, the two methods and the discussions about remaining uncertainties are very similar. Referring to the importance of turbulent fluxes, Foken et al. (2009) gives a concise overview about the difficulties of complete closures of fluxes. Measuring fluxes means to be aware of contributions that might not be accurately captured, and to minimize them by suitable methods and measuring strategies, which includes the choice of suitable meteorological conditions. In some convective situations, also the vertical flux above the source has to be considered. When dealing with distinct sources in a limited area, where deposition, storage and other terms can be neglected, we have the following situation:

Since the wind field is not homogeneous in the vertical, the conceptual model described in Fig. 2 can either be applied on different layers, or the "wind vectors" and the "concentrations" are already multiplied and averaged in the vertical. The second interpretation is more adequate, because the first one raises the question of what happens if a parcel of air changes its altitude, and hence the layer. The general statement is, that the inflow and outflow of background concentrations is balanced (sum = zero), and only the additional fluxes added to the background by known (and unknown) sources in the "box" are of interest.

Instead of a box or cylinder around the source, we put a virtual box downwind of the source(s) according to Fig. 3 and 4.

Atmos. Meas. Tech. Discuss., doi:10.5194/amt-2016-362, 2016
Manuscript under review for journal Atmos. Meas. Tech.
Published: 25 November 2016

Atmospheric Measurement Techniques Discussions

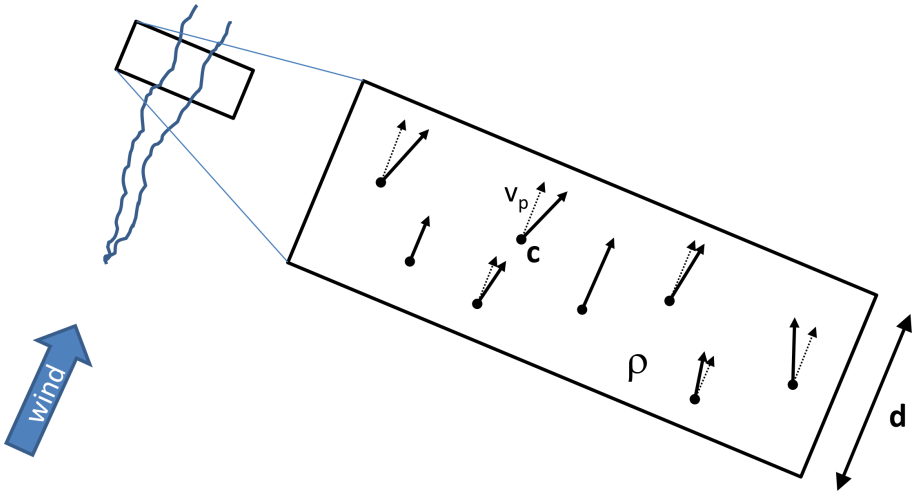

Figure 3. Instead of a vertical cross-section with infinitesimal thickness, a "wall" with a defined thickness d, where the cross section was flown, was observed with the in-situ measurements. The individual fluxes are calculated from individual wind vectors and concentrations in turbulent resolution (5 Hz). In order to get a spatial distribution of the fluxes this "wall" is divided in grid cells (see Fig, 4).

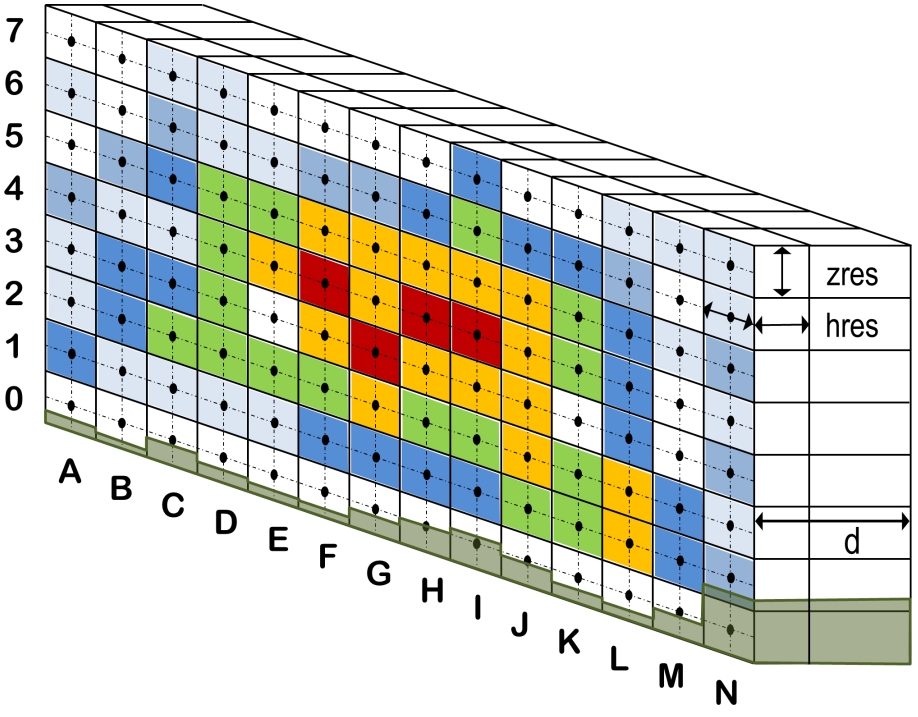

Figure 4. The vertical cross section of Fig. 3. Grid cells containing data are coloured (red denotes high concentrations, blue denotes low concentrations) and cells with no data are left blank

Atmos. Meas. Tech. Discuss., doi:10.5194/amt-2016-362, 2016
Manuscript under review for journal Atmos. Meas. Tech.
Published: 25 November 2016

Atmospheric Measurement Techniques Discussions

This "wall" has a certain depth, and was observed for a given amount of time. The fluxes through each "brick" of that wall (a grid with vertical and horizontal spacing according to Fig. 4) are calculated in a straight forward manner: Each measurement of an instantaneous flux (concentration times perpendicular component of the wind) is regarded as a sample, and averaged in each grid cell. It is important to note that this includes both the "mean advective fluxes", and the "turbulent fluxes". For the case where turbulent fluxes occur (both horizontally and vertically from neighbouring grid cells), this approach includes such events. Potentially we would obtain similar results when multiplying average concentrations with average winds per grid cell. However, the fully resolved approach is more appropriate (i.e. more complete), because possible co-variances are included. If lower concentrations are associated with lower wind speeds, and vice versa, a real (turbulent) flux is present. However, when concentrations and winds are averaged first, this turbulent flux would not be detected. With the remote sensing approach discussed in Krings et al. (2011, 2013), the turbulent fluxes are indirectly included when fitting the column concentrations to a Gaussian plume model. Note that the in-situ method described here does not assume the shape of the plume. It utilizes knowledge of the statistics about parcels of air crossing an imaginary border. The assumptions and the consequences when they are violated are discussed below. Average concentrations per grid cell were calculated in order to plot these fields for the cross-sections. Concentration fields were calculated as absolute concentrations, and as net concentrations, with the background concentrations subtracted. How the background concentrations were calculated is described below.

The positions of the cross-sections were selected based on the flight patterns (minimum and maximum distance), and the mean wind direction. The angle of the cross-section was adjusted for a cross-wind component of $0.1\,\mathrm{m\,s^{-1}}$ or less, and the width of the cross section should include enough background concentrations.

Figures 3 and 4 are used to explain the steps of the processing. Based on the flight track on the map, the minimum and maximum distance from the source was defined. The difference of these distances is the thickness of the wall, shown as "d" in Fig. 3 and 4. The orientation of the wall is adjusted until the amount of the average crosswind component is $0.1\,\mathrm{m\,s^{-1}}$ or less. Larger crosswind components would not be a problem (see Sect. A). However, it makes sense to adjust the cross section perpendicular to the average wind direction. In a second step, the lateral boundaries are chosen. They should be clearly outside of the plume, but not too far away since this would increase the uncertainty about the background concentration. The wider the cross section the more likely secondary sources are included in the flux calculation (see below, when discussing the background).

The horizontal and vertical resolutions *hres* and *zres* were either $100\,\mathrm{m}$ or in case of sparse data $200\,\mathrm{m}$. All calculations were done in vertical columns of *hres* $\times$ *hres*, i.e. all the measurements within d - which is in in the order of a few hundred meters - were projected onto a wall of thickness *hres*. In the vertical, the grid spacing was *zres*. Therefore, the calculations were done in grid cells with the dimension *hres* $\times$ *hres* $\times$ *zres*, using data in the volumes *hres* $\times$ d $\times$ *zres*. In Fig. 4, all grid cells containing data are coloured and cells with no data are left blank. The algorithm that interpolates the cross section begins on the top level, where measurements might be sparse. In the example shown, the cells E7 to H7 and J7 to K7 are interpolated linearly, where A7 to B7 would be kept at the value of C7. Missing values in E3 and K3 are interpolated vertically from neighbouring grid cells E2/E4 and K2/K4 respectively. The same for A5, M3, M4 and M6.

Atmos. Meas. Tech. Discuss., doi:10.5194/amt-2016-362, 2016
Manuscript under review for journal Atmos. Meas. Tech.
Published: 25 November 2016

Atmospheric Measurement Techniques Discussions

The linear interpolations and extrapolations were sufficient for filling the grids (mainly for graphical reasons), because our focus was on measured data, and the results should not depend too much from interpolations and extrapolations.

Usually there was a gap between the lowest flight track, and the surface (taken from SRTM). The maximum of the digital terrain model (DTM) below the flight track was taken as the terrain elevation below the column. The different parameters were treated differently.

Concentrations were kept constant in the grid cells below the lowest flight track. This might result in an overestimation for CO_2. However, this is not very relevant, and we just do not have more accurate information. Compare also the comment concerning fluxes.

Masses for column concentrations are proportional to the gap, i.e. in cell C0 in Fig. 4, about 55% of the mass of cell C1 is taken.

The wind is zero below the DTM. However, the fluxes above the surface are taken from the layer above. For CO_2 this is often not relevant, since the plumes for example from power plants do not reach the surface close to the source, and it is possible to fly in the background concentrations below the plume.

Extrapolation above the highest flight track: In cases, where the "curtain" flown did not reach the top of the plume extrapolation above the highest track is applied.

The background concentrations were assumed to be the minimum concentrations in each layer (1 to 7 in Fig. 4). It is clear that the background is not just one concentration for all altitudes. However, it is clear that this is a sensitive parameter. Taking the minimum per layer means that any enhancement above this lowest possible background concentration is considered to be a flux from the source(s) under study. However, concentrations exceeding the background could also be caused by sources far away, or convective mixing in the boundary layer. Taking the minimum tends to overestimate the local fluxes.

However, in this case study, where the sources were close together, and the background concentrations had to be taken very close to the plumes, the contrary is true: There is a tendency to overestimate the locally contaminated background. On the other hand, the enhanced concentrations in the plumes were very pronounced in this case. These and other contributions to uncertainties are discussed below.

4.2 Discussion about main uncertainties in-situ

4.2.1 Measurement errors

The wind components (u, v, w) have an accuracy of $0.5\,\mathrm{m\,s^{-1}}$ each, the CO_2 concentrations have an accuracy of better than 1 ppm, and the CH_4 of better than 5 ppb. However, as the background concentrations are subtracted, the absolute concentrations are not important, resulting in uncertainties in terms of precision (stability of the sensitivity within an hour) instead of absolute accuracies, which leaves us with maximum uncertainties of 0.5 ppm for CO_2 (using the two CO_2 instruments in combination with flask samples) and 2 ppb for CH_4. The uncertainties of the wind measurements remain in the order of $0.5\,\mathrm{m\,s^{-1}}$. The main uncertainty is the crosswind component relative to the aircraft. However, when flying back and forth through any plume on a similar altitude, then this error is averaged out. Nevertheless, we make a coarse error assessment with these numbers.

Atmos. Meas. Tech. Discuss., doi:10.5194/amt-2016-362, 2016
Manuscript under review for journal Atmos. Meas. Tech.
Published: 25 November 2016

Atmospheric Measurement Techniques Discussions

Then the relative error based on the wind measurement is 10% at wind speeds in the order of $5\,\mathrm{m\,s^{-1}}$, increasing with weaker winds, and decreasing with higher wind speeds. For CO_2, a plume with moderate 50 ppm above background only adds another percent, and the uncertainty of the excessive CH_4 is in the order of one permille. In the case discussed here, wind speeds were around $8\,\mathrm{m\,s^{-1}}$, with excessive CO_2 concentrations of more than 100 ppm (see Fig 5), leading to the conclusion that the error for horizontal fluxes due to the uncertainties of the primary measurements is clearly below 10%.

4.2.2 Other sources for errors

The accuracy and precision discussed above are important, however, not the main criterion for reliable flux estimates. It is just the "conditio sine qua non". Only under unrealistically ideal conditions, where winds and concentrations over the whole cross sections could be captured completely and instantaneously, and could be repeated many times, the remaining uncertainties would arise from the (systematic) measurement errors. These are, as discussed above, quite small. However, as already mentioned in Sect. 4.1, and discussed in similar work referenced there, other reasons for uncertainties can be dominating, which are hard to quantify. The approach here was to vary the assumptions and parameters used in the calculations in a wide range. This sensitivity analysis allowed comparing the methodological variations with the average fluxes.

The main uncertainties are dependent from the meteorological conditions and the flight patterns. An ideal flight pattern is covering the plume as completely as possible. For the CO_2 plumes, the minimum height of 50 m or even more above ground is generally not a problem when measuring sufficiently close to the sources, because emissions were originating from high chimneys. For the extrapolation to the surface, the concentrations are kept constant (see Fig. 5), and the wind is linearly reduced to zero at the surface (a logarithmic wind profile would cause a higher risk for an overestimation of the fluxes). Due to reasons discussed above, when explaining the method with the "gridded wall", it is clear that the wall should be as thin as possible, because otherwise, artefacts could occur. In this case, the flight pattern was not ideal due to air space restrictions. Also the wind direction was not ideal, because some of the four point sources were nearly collinear. Nevertheless this case was chosen, because the conditions for the remote-sensing (clear sky) were best. Therefore, the uncertainties for the in-situ measurements discussed here are worst-case, and should not be generalised.

Another source of uncertainty is instationarity, i.e. varying source strengths from day to day, or even by the hour, while the measurements account only for the emissions for the time of the overflight. Another type of instationarity is caused by the atmospheric turbulence on the scale of a few hundred meters, where a maximum concentration (puff instead of continuous plume) can be missed, or captured by coincidence, and therefore overestimated in the average. Generally spoken, the 4-d inhomogeneities cannot be captured in a "snapshot". This effect can only be minimised with repeated, dense flight tracks. Another issue is the definition of the boundary layer. In an ideal case, cross sections are flown to an altitude, where no excessive concentrations are detected anymore, i.e. where the plume is confined below. Also this was not ideal at the day of this case study, because the convective atmospheric boundary layer was higher than it was possible to complete the cross sections due to air space restrictions.

Since a deductive error estimate as it is possible for the basic measurements is not possible for the overall flux result, a sensitivity analysis was applied to all cases. In this case study, the five individual cross sections with fluxes were calculated using

Atmos. Meas. Tech. Discuss., doi:10.5194/amt-2016-362, 2016
Manuscript under review for journal Atmos. Meas. Tech.
Published: 25 November 2016

Atmospheric Measurement Techniques Discussions

nine sets of parameters. The lower limits for the fluxes were found by applying no extrapolation at all. Then the extrapolation to the surface was added, which only contributed a few percent of the fluxes in four of the five cross sections, and finally an extrapolation up to 1400 m a.m.s.l. (above mean sea lavel, estimated top of the convective boundary layer based on profiles shown in Fig. 9 and 10). These three cases were calculated with vertical and horizontal grid resolutions of 50, 100 and 200 m, where the 100 m were standard (best adapted to the typical vertical distance between flight tracks). This led to a sensitivity study where the medians per cross section were taken as the result and the second lowest and the second highest values (something like 10- and 90-percent percentiles) were considered as the "error bars". This led to uncertainties in the order of $\pm 28\%$ for the worst cross section (big gap between the lowest track, and the surface), and $\pm 10\%$ for the best. They are combined when sums or differences of cross sections are calculated when trying to separate the different sources. However, the total was measured in one single cross section which included the three major sources, i.e. the same total as in the results from the remote-sensing.

4.3 Fluxes from remote sensing greenhous gas information

The processing of the MAMAP remote sensing data is based on the methods described by Krings et al. (2011, 2013). A modified version of the Weighting Function Modified Differential Optical Absorption Spectroscopy (WFM-DOAS) algorithm (Buchwitz et al., 2000) is used to obtain vertical column information of CH_4 or CO_2. It relies on a least squares fit of the logarithmic simulated radiance spectrum to the measurements after correction for dark signal and pixel-to-pixel gain. Additionally a look-up-table approach has been implemented accounting for varying solar zenith angle (SZA) and surface elevation. The conversion from total columns to column averaged dry air mole fractions (XCH_4, XCO_2) is performed using the proxy method, assuming that locally CH_4 is sufficiently constant to compute XCO_2 (or vice versa for XCH_4). This method is suitable for point sources as the case in this study.

Emission rate estimates are then obtained using an inverse Gaussian plume model fitting flux and atmospheric stability. In a second approach mass balance estimates are computed leading to two independent inversion methodologies with the exception of wind information which is taken from the routine analysis of the numerical weather prediction model COSMO-DE (Doms, 2011) and the in-situ turbulence probe of the DIMO aircraft which is used for both methods.

For more details regarding the inversion approaches see Krings et al. (2011, 2013).

5 Results

5.1 In-situ

The results of the in-situ flux analysis are shown in Table 1. The median of the nine methods of calculation as described above for the total emission flux is 49.0 $\mathrm{MtCO_2 yr^{-1}}$, from which 79.1% was measured directly, which means that 20.9% is determined from the linear extrapolation to the surface. The lower estimate (without any extrapolation, which is unrealistic) is at 43.7 $\mathrm{MtCO_2 yr^{-1}}$, and the "best estimate" including an extrapolation to the top of the well mixed boundary layer at 1400 m a.m.s.l. is at 61.2 $\mathrm{MtCO_2 yr^{-1}}$. The low, median and high estimates for the single source Niederaußem are 20.6, 24.0 and

Atmos. Meas. Tech. Discuss., doi:10.5194/amt-2016-362, 2016
Manuscript under review for journal Atmos. Meas. Tech.
Published: 25 November 2016

Atmospheric Measurement Techniques Discussions

Table 1. Error analysis for in-situ flux estimates based on different extrapolation scenarios and varying grid resolution (see Sect. 4.2.2). The emission rate for Neurath new and old blocks was derived from the difference between Niederaußem and total.

Power plants	Low estimate [$MtCO_2/yr$]	Median [$MtCO_2/yr$]	High estimate [$MtCO_2/yr$]
Niederaußem	20.6	24.0	26.7
Neurath (new and old blocks)	23.1	25.0	34.5
Total	43.7	49.0	61.2

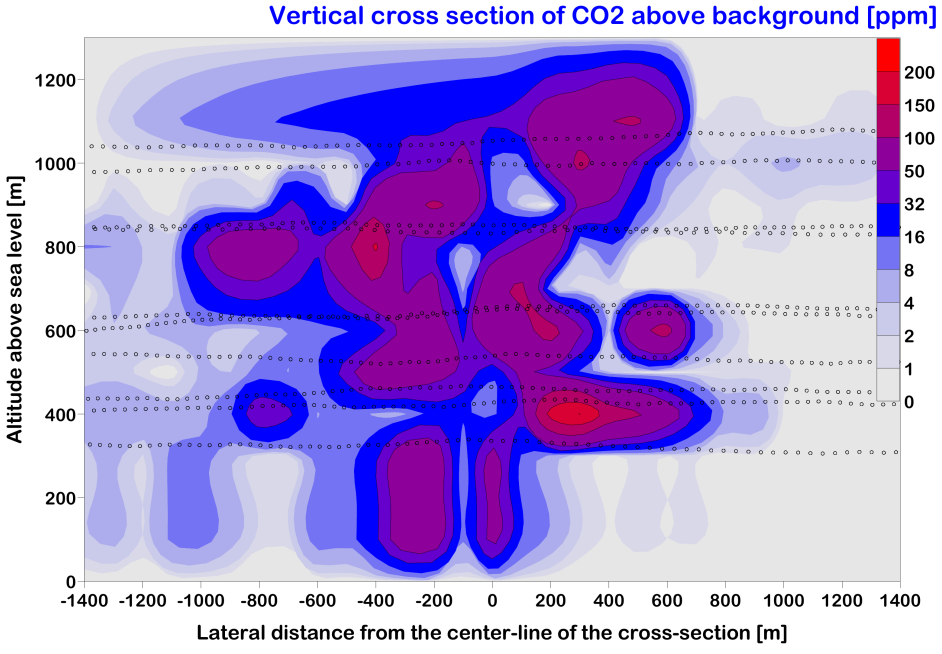

Figure 5. Interpolated and extrapolated CO_2 concentrations measured in-situ downwind of Niederaußem power plant.

$26.7\,MtCO_2yr^{-1}$ respectively, whereas the two collinear sources Neurath new and old, which could not be separated in a reliable manner, led to an estimate of $25.0\,MtCO_2yr^{-1}$ (23.1 to 34.5).

Two days later, where the conditions were more favorable in terms of wind direction and better defined top of the mixed boundary layer, slightly higher values and narrower error margins were found, while the reported emissions were 10% lower, indicating that the sub-optimum conditions on August 15 led to an underestimation, however, with realistic minima and maxima according to the sensitivity analysis.

Atmos. Meas. Tech. Discuss., doi:10.5194/amt-2016-362, 2016
Manuscript under review for journal Atmos. Meas. Tech.
Published: 25 November 2016

5.2 Remote sensing

5.2.1 Measurement data

The column averaged dry air mole fractions of CO_2 were retrieved using CH_4 as a light path proxy: $XCO_2(CH_4)$. The corresponding background profiles for the linearization points use the U.S. standard atmosphere (U.S. Committee on Extension to the Standard Atmosphere, 1976) scaled to actual values. In this case, background XCO_2 was set to 390 ppm based on in-situ data upwind of the power plants in the boundary layer and results from the SECM model (Reuter et al., 2012) above. The methane background XCH_4 was estimated to about 1.805 ppm also based on in-situ measurements in the upwind area of the boundary layer scaling the standard atmosphere. An assumed uncertainty of the ratio of the background columns of 1% accounts for possible deviations from these values. The spectroscopic data base used for the computation of absorption cross sections was HITRAN 2012.

Aircraft altitude during the measurements was almost constant at about 1590 m (+/- 25 m), which was also selected for the reference radiative transfer. Assuming a constant aircraft velocity of 200 km/h, the ground scene size is about 22 m x 54 m (cross track × along track) for the installed optical front telescope. Thereby the along track ground scene size describes the full width at half maximum for the sensitivity along the flight track. During the measurement, the solar zenith angle varied from about 37.5° to 45.3°.

The radiative transfer model was interpolated using a two dimensional look-up table (LUT) based on solar zenith angle and surface elevation. For that the SRTM digital elevation model (Shuttle Radar Topography Mission (SRTM) version 2.1, http://dds.cr.usgs.gov/srtm/version2_1/, a collaborative effort from NASA, NGA as well as the German and Italian Space Agencies) was used. Due to the changing measurement geometry, the conversion factor to correct for the altitude sensitivity effect (Krings et al., 2011) has to be determined for each measurement independently using also a LUT. This correction takes into account that light passes twice below the aircraft where the observed plumes are located. On average, the conversion factor for the present measurements is about 0.49.

5.2.2 Quality filtering

Filtering, based on the fit quality, has been applied rejecting measurements with a root mean square value of the differences between measurement and model after the fit (see Fig. 6) larger than 0.9%.

An additional filter has been applied dependent on the signal strength to avoid measurements close to saturation (more than ≈90% detector filling) and in the lower signal to noise range, e.g., over water which has a lower surface spectral reflectance in the short-wave infrared. Measurements with a detector filling of less than about 20% (13000 counts) appear to have a slight signal dependency (Fig. 7) and were neglected for the inversion process. Furthermore to ensure nadir viewing geometry the deviation from the vertical was not allowed to exceed 5°.

The $XCH_4(CO_2)$ precision after filtering is approximately 0.29% determined from the standard deviation of the data outside the plume area.

Atmos. Meas. Tech. Discuss., doi:10.5194/amt-2016-362, 2016
Manuscript under review for journal Atmos. Meas. Tech.
Published: 25 November 2016

Atmospheric Measurement Techniques Discussions

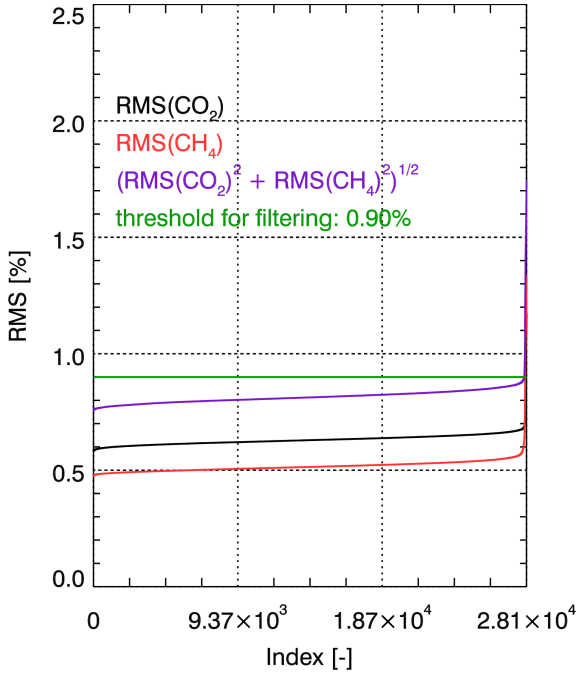

Figure 6. Fit quality of the retrievals ordered by value of the root mean square (RMS) value of the difference between fit and measurement. The green horizontal line denotes the filter threshold.

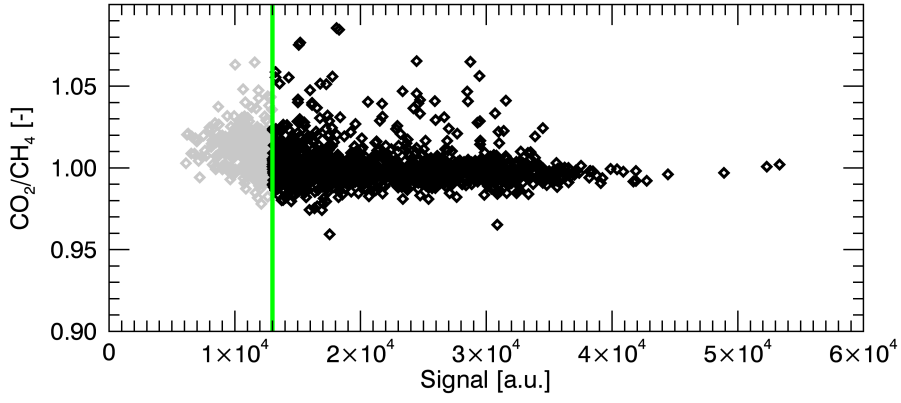

Figure 7. Averages of the profile scaling factor ratios of CO_2/CH_4 versus the maximum signal. The measurements displayed in grey left of the green vertical line denoting the signal threshold of 13000 counts are excluded from the data. The increased values with respect to the main distribution are due to the actual CO_2 plumes. The ratios have not been corrected for the altitude sensitivity (Sect. 5.2.1) and do therefore not denote XCO_2.

Atmos. Meas. Tech. Discuss., doi:10.5194/amt-2016-362, 2016
Manuscript under review for journal Atmos. Meas. Tech.
Published: 25 November 2016

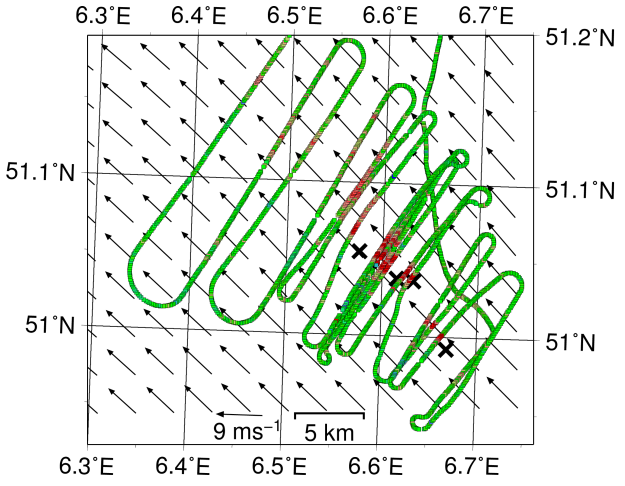

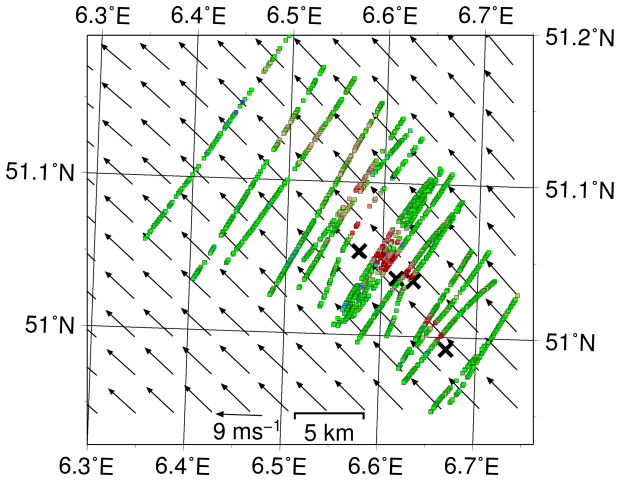

Figure 8. Qualitative MAMAP remote sensing XCH_4 data unfiltered (left) and the cross sections filtered as described in the main text (right). The crosses denote the power plant locations (see Fig. 1). Arrows denote wind vectors from the COSMO-DE model at an altitude of about 350 m above sea level (model layer 45) at 13:00 UTC.

Fig. 8 shows the $XCO_2(CH_4)$ data acquired over the coal fired power plants without and with the filtering applied. Clearly visible are the overlapping CO_2 plumes originating at the individual power plant locations and advected in downwind direction towards North-West in agreement with the wind field as computed by the COSMO-DE model.

5.2.3 Atmospheric conditions and wind information

A fundamental parameter for the inversion is wind speed. To compute an average wind speed throughout the CO_2 plume from model and in-situ data also the boundary layer depth is important.

Fig. 9 shows the in-situ and COSMO-DE result for temperature and virtual potential temperature for the model grid point about 1.5 km North of Neurath power plant in the centre of the main plume area. In a first approximation the boundary layer depth can be identified by a sharp increase in virtual potential temperature. While in the COSMO-DE model data there appears to be a weakly developed boundary layer evolving from about 400 m altitude at 11:00 UTC to about 800 m at about 14:00 UTC there is no indication in the in-situ virtual potential temperature data that the transition to the free troposphere is located in the lower 1100 m. The aerosol distribution is also not conclusive in this respect. This is because a sharp decrease at the transition to the free troposphere might be expected. This is furthermore confirmed by the fact that there are enhanced CO_2 amounts throughout the probed altitude layers (see Fig. 10). Consequently it can only be concluded that the boundary layer depth is likely larger than 1100 m. For the analysis a boundary layer depth of 1500 m was assumed (with uncertainty estimates for cases of 1200 m and 1800 m, see Sect. 5.2.5).

Modelled and measured wind direction are similar in lower altitudes but agree less well at higher altitudes and later times. However, the wind direction is derived from the remote sensing data directly without using the model information.

Atmos. Meas. Tech. Discuss., doi:10.5194/amt-2016-362, 2016
Manuscript under review for journal Atmos. Meas. Tech.
Published: 25 November 2016

Atmospheric Measurement Techniques Discussions

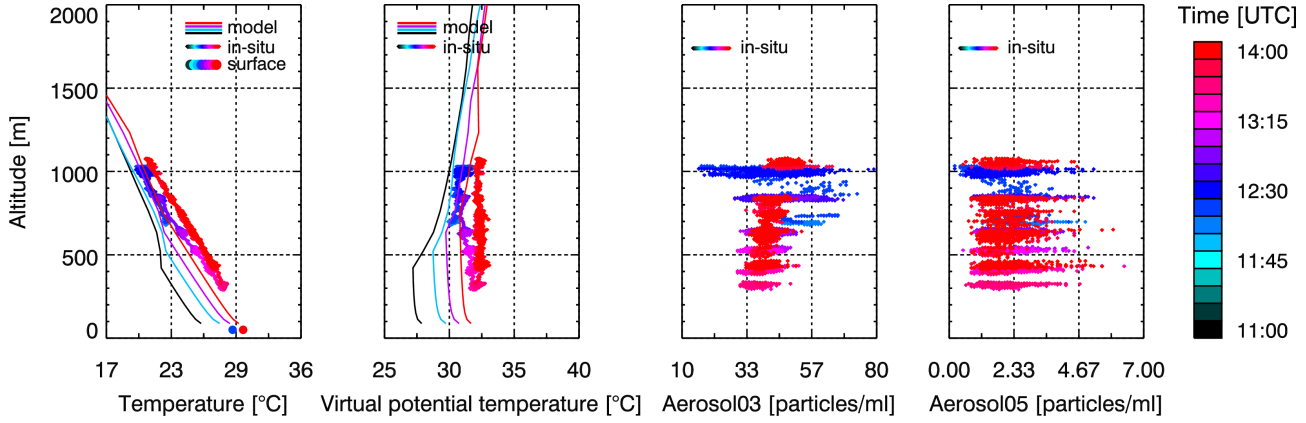

Figure 9. From left to right, in-situ data of temperature, virtual potential temperature, aerosol particles larger than 0.3 µm and aerosol particles larger than 0.5 µm. For temperature and virtual potential temperature also the COSMO-DE model result is shown and for the temperature additionally ground based in-situ data from Düsseldorf airport which is approximately 30 km NNE of Neurath power plant.

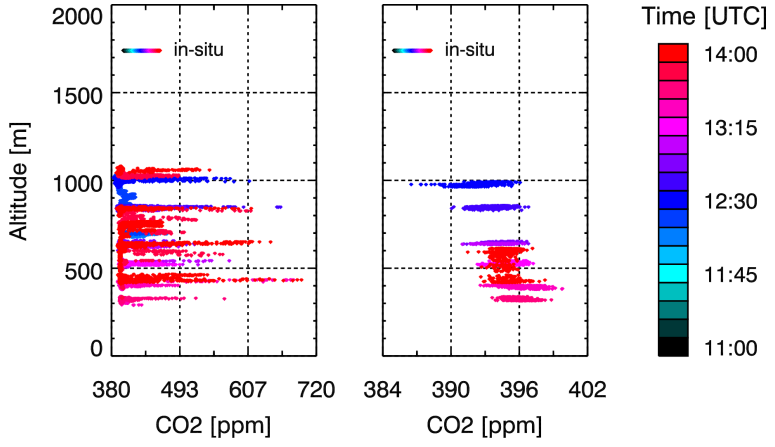

Figure 10. Airborne in-situ measurements of CO_2 in the whole measurement area (left) and upwind of the plume (right).

Figure 11 shows wind speed and direction for the same model grid point. The measured in-situ wind speed averaged over 60 s ranges from about 7 $\mathrm{m\,s^{-1}}$ to 11 $\mathrm{m\,s^{-1}}$ for the time and altitude range of the overflight and is rather constant with altitude. Altitudes covered by in-situ measurements range from about 300 m to 1100 m a.m.s.l.

Since in-situ wind information is not always available in time and space where remote sensing measurements are taken, the in-situ wind data is used to calibrate the COSMO-DE model result in the measurement area during the time of the remote sensing overflights.

The precision of the wind model was estimated to about 0.9 $\mathrm{m\,s^{-1}}$ (1 σ) with negligible bias for the case described in Krings et al. (2011). Assuming the same error holds in the present study, this leads to a wind based relative error (1 σ) on the inversion of about 10%.

Atmos. Meas. Tech. Discuss., doi:10.5194/amt-2016-362, 2016
Manuscript under review for journal Atmos. Meas. Tech.
Published: 25 November 2016

Atmospheric Measurement Techniques Discussions

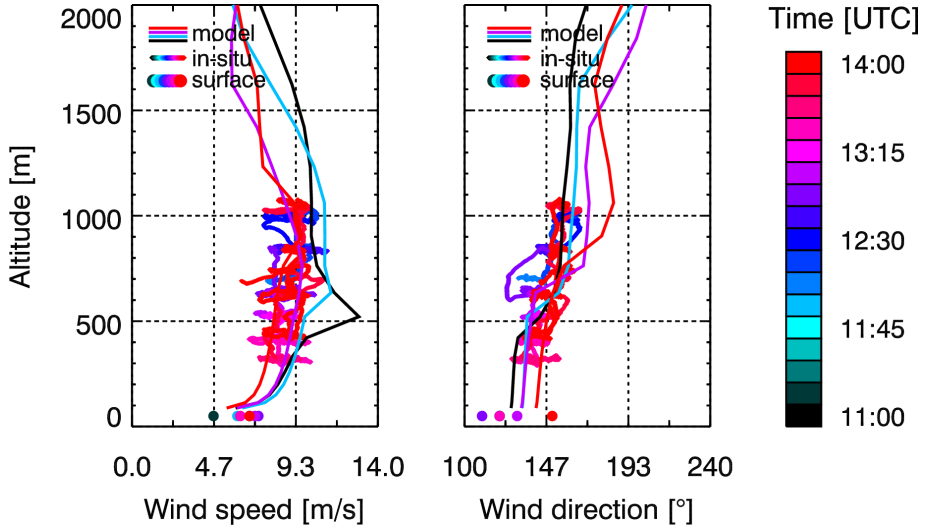

Figure 11. Wind speed (left) and direction (right) as measured from the in-situ turbulence probe as well as COSMO-DE model data.

Table 2. Comparison of modeled and measured wind speed for several altitude layers.

Altitude range a.m.s.l. [m]	Model wind speed [$m\,s^{-1}$]	In-situ wind speed [$m\,s^{-1}$]	Wind speed difference (in-situ - model) [$m\,s^{-1}$]	Relative wind speed difference (in-situ - model)/model [%]
291 – 440	8.99	8.53	-0.46	-5.1
440 – 588	9.33	8.47	-0.86	-9.2
588 – 737	9.48	8.53	-0.95	-10.0
737 – 885	9.84	9.11	-0.74	-7.5
885 – 1034	9.27	9.40	+0.13	+1.4
			Average: -0.58$m\,s^{-1}$	Average: -6.1%

This error can be reduced when on site wind information is available, for example, from airborne turbulence measurements as they were used in Krings et al. (2013) and that were also performed during the present campaign.

Figure 12 shows the flight pattern of the in-situ measurements. The measurements concentrate on transects at several altitude layers around the two Neurath power plants and around the extended area including Frimmersdorf power plant.

To quantify the difference between measured and modeled wind speed, the probed altitude range has been divided into 5 equally thick layers in which the deviation between the in-situ measurements on the one hand and the associated model data interpolated in time and space on the other hand were computed and subsequently averaged over the altitude layers.

Atmos. Meas. Tech. Discuss., doi:10.5194/amt-2016-362, 2016
Manuscript under review for journal Atmos. Meas. Tech.
Published: 25 November 2016

Atmospheric Measurement Techniques Discussions

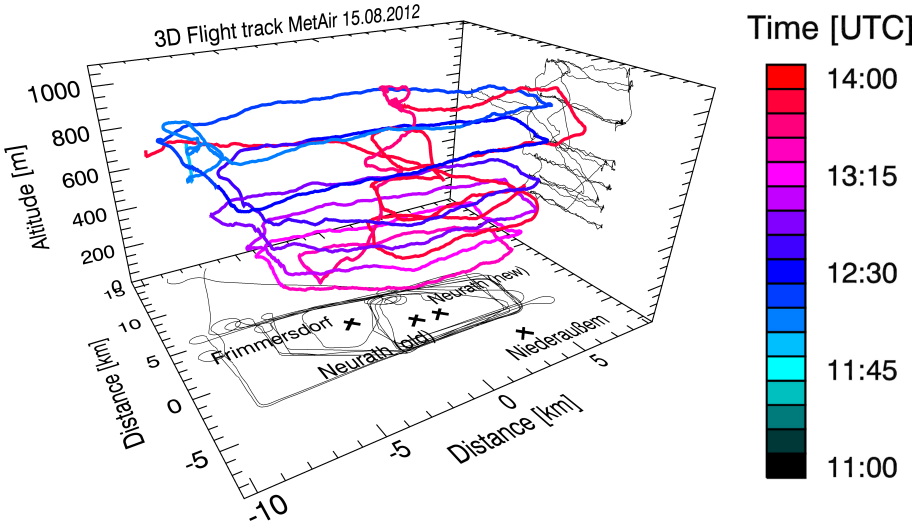

Figure 12. 3D representation of the in-situ flight track. Also shown are projections on the ground and on a vertical plane for better interpretation.

For the available model and measurement data from the target area and time, this yields an average overestimation of about $0.58\,\mathrm{m\,s^{-1}}$, i.e. about 6.1%. This is well within the approximate error of about $0.9\,\mathrm{m\,s^{-1}}$. Similar to Krings et al. (2013) the in-situ wind error of $0.5\,\mathrm{m\,s^{-1}}$ is assigned to the calibrated wind.

The complete results are shown in Table 2. Note that the results do not directly relate to Fig. 11 which only shows the model wind speed at one specific COSMO-DE grid point while model wind data from the whole measurement area enters the computations in Table 2.

5.2.4 Inversion for emission data

Preparation and performance of the Gaussian plume inversion and the integral inversion method is very much in line with Krings et al (2011, 2013). Since the inversion proved to be extremely stable no a priori information on emission rate or stability were required simplifying the cost function to be minimised in the iterative inversion process.

The data were gridded to pixels of $35\,\mathrm{m}$ x $35\,\mathrm{m}$ having approximately the same area as the MAMAP ground scene size. The impact of different pixel sizes for the gridding is assessed in Sect. 5.2.5. No additional smoothing was applied. Note that the gridding was not used for the mass balance method.

Prior to the inversion the data were normalised dividing by the regional background. Since the measured area and time is somewhat larger than in the previous studies, no constant normalisation was selected but a track by track procedure that is also able to account, for example, for linear gradients that are unrelated to the source. Thereby data from each cross section (see Fig. 8) is normalised by a linear function that is determined by the flanks of the track excluding the plume area. If the track does not measure sufficient data outside the plume, then this method results in an underestimation of emissions. Because of

Atmos. Meas. Tech. Discuss., doi:10.5194/amt-2016-362, 2016
Manuscript under review for journal Atmos. Meas. Tech.
Published: 25 November 2016

Atmospheric Measurement Techniques Discussions

that and because gaps due to filtering are rather large from track 10 onwards, only the first 9 downwind tracks with respect to Niederaußem power plant have been included in the analysis so that emission from Frimmersdorf were not determined in this approach.

Obtaining an adequate estimate of the mean wind speed with which the emitted gas is transported is challenging when there are serveral sources which are separated in downwind direction. Naturally, the relative emission rates of the sources will generally not be known before the data analysis. Therefore the weighting of the wind profile according to the significant altitude layers is not trivial. In the present case the low variability of wind speed with altitude (see Fig. 11) however makes the estimation less sensitive to errors in this regard. The mean wind speed was estimated assuming Niederaußem power plant, the power plant that is located most downwind of all emitters, as the only source. The emitted CO_2 was then distributed using a vertical Gaussian dispersion with the stability parameter resulting from the inversion of the 2D Gaussian plume inversion model. This information could be used to obtain an altitude weighted mean wind speed for the remote sensing cross sections through the plume. The cross section wind speeds were used individually for the mass balance approach and averaged for the inverse plume model over the relevant area. Boundary layer top height (represented as a reflective layer as in Turner (1970)) and emission height needed for the vertical dispersion were varied around the baseline parameters to estimate the range of errors resulting from these assumptions (see Sect. 5.2.5).

Wind direction was determined from the measured remote sensing data to about 147.5° by both visual inspection and minimizing the stabiliy parameter (see also Sect. 5.2.5). When fitting the stability parameter to the retrieved XCO_2 this yields a=214.0 ($\pm 8.8\%$ statistical error), i.e. stability class A (very unstable atmospheric conditions, Martin (1976); Masters (1998)), independent of wind speed.

Using this stability as input for a vertical Gaussian dispersion model as a function of distance to the source to compute a weighted mean of the wind profile, an average wind speed of $8.2\,\mathrm{m\,s^{-1}}$ was obtained for the plume area covered by the first 9 downwind tracks of the MAMAP data. For this the in-situ calibrated wind model data was used.

Applying this wind speed to the Gaussian plume inversion, the result for the average emission rate for the time of the overflight is in total about $63.6\mathrm{MtCO_2yr^{-1}}$ ($\pm 3.0\%$ statistical error) split into $24.0\mathrm{MtCO_2yr^{-1}}$ ($\pm 4.6\%$), $14.2\mathrm{MtCO_2yr^{-1}}$ ($\pm 6.3\%$) and $25.4\mathrm{MtCO_2yr^{-1}}$ ($\pm 5.2\%$) for the power plants Niederaußem, Neurath new and Neurath old, respectively. As mentioned before the evaluated tracks are all located upwind of power plant Frimmersdorf. Therefore no emission rate for Frimmersdorf was derived. The contour lines as an overlay on the retrieved XCO_2 can be seen in Fig. 13.

For the mass balance approach a wind speed was computed for each individual track ranging from about $8\,\mathrm{m\,s^{-1}}$ to $9\,\mathrm{m\,s^{-1}}$. Similar to the inverse plume model, the first 9 downwind tracks were analysed and the associated cross sections are shown in Fig. 14. The data were normalised for each flight track individually using a linear fit based on the data outside the plume. This was applied in order to account for local gradients or other offsets. The definitions of the outside plume area are listed in Table 3.

The results are shown in Fig. 15 for the individual tracks and the average emission in-between power plants. Figure 15 also shows that there is basically no CO_2 influx from upwind into the measurement area.

Atmos. Meas. Tech. Discuss., doi:10.5194/amt-2016-362, 2016
Manuscript under review for journal Atmos. Meas. Tech.
Published: 25 November 2016

Atmospheric Measurement Techniques Discussions

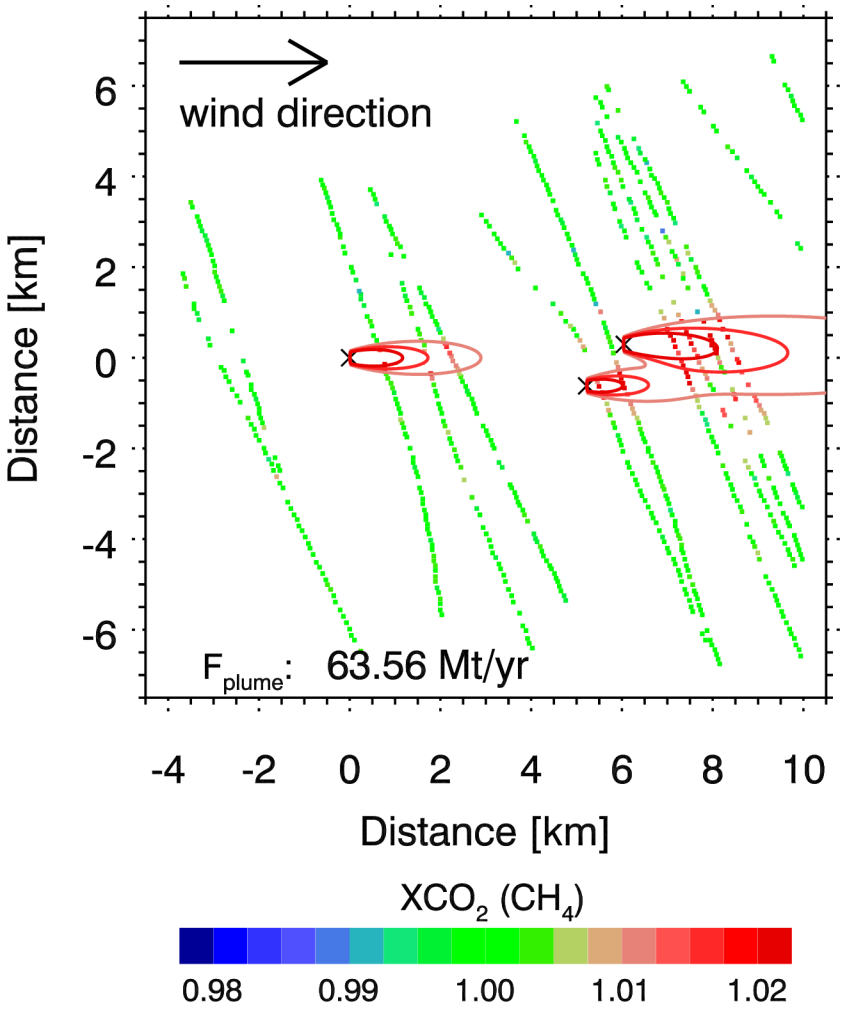

Figure 13. Gridded MAMAP XCO_2 results rotated so that wind direction points into positive x-direction and contour lines of the inferred plume models for the individual power plants. Total emission rate is 63.6 $\mathrm{MtCO_2 yr^{-1}}$ for the time of the overflight. Ground scenes are shown slightly enlarged for better visiblity.

Table 3. Normalisation distances to the end of the measurement track for each individual remote sensing transect.

Track	Distance to end of track	Comment
Upwind, Downwind #3 – #5	2000 m	Baseline normalisation length for shorter tracks
Downwind #1	3000 m	Avoid measurements with increase in CH_4 next to plume
Downwind #2	1500 m	Plume not centered on track
Downwind #6 – #9	3000 m	Track lengths increased and wider plume further downwind

Atmos. Meas. Tech. Discuss., doi:10.5194/amt-2016-362, 2016
Manuscript under review for journal Atmos. Meas. Tech.
Published: 25 November 2016

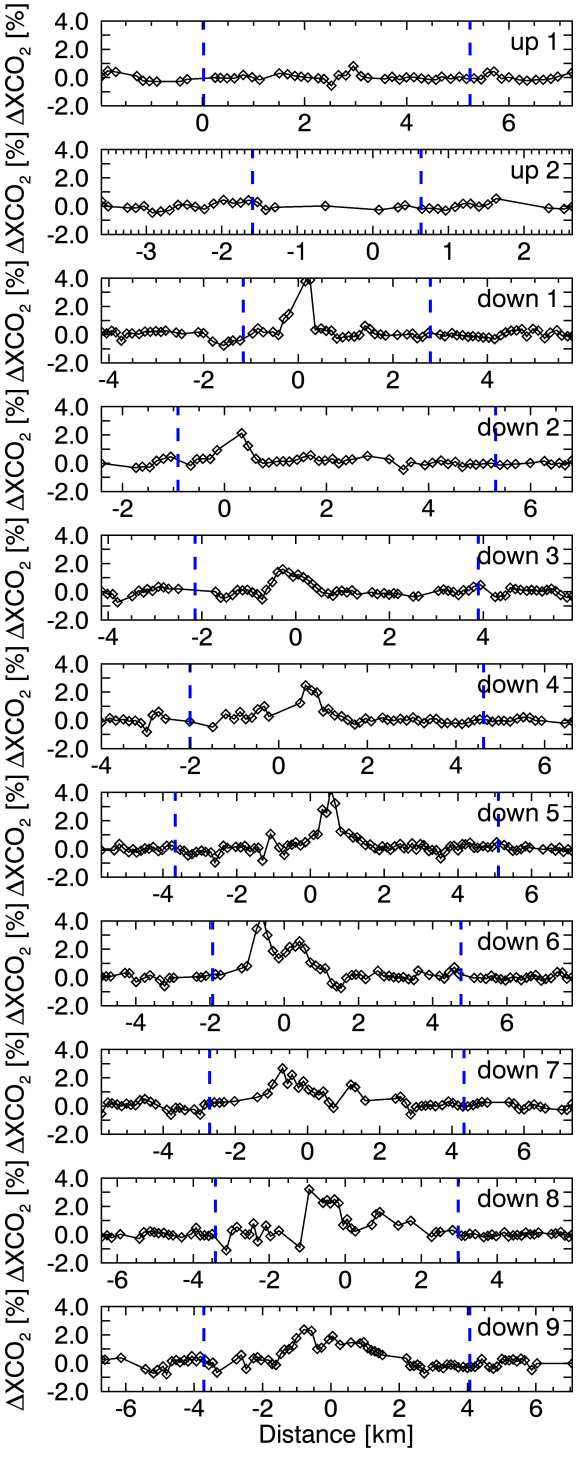

Figure 14. MAMAP XCO_2 cross sections for the tracks used for the emission rate estimates. The area outside the dashed vertical lines denote the data that were used for the normalisation.

Atmos. Meas. Tech. Discuss., doi:10.5194/amt-2016-362, 2016
Manuscript under review for journal Atmos. Meas. Tech.
Published: 25 November 2016

Atmospheric Measurement Techniques Discussions

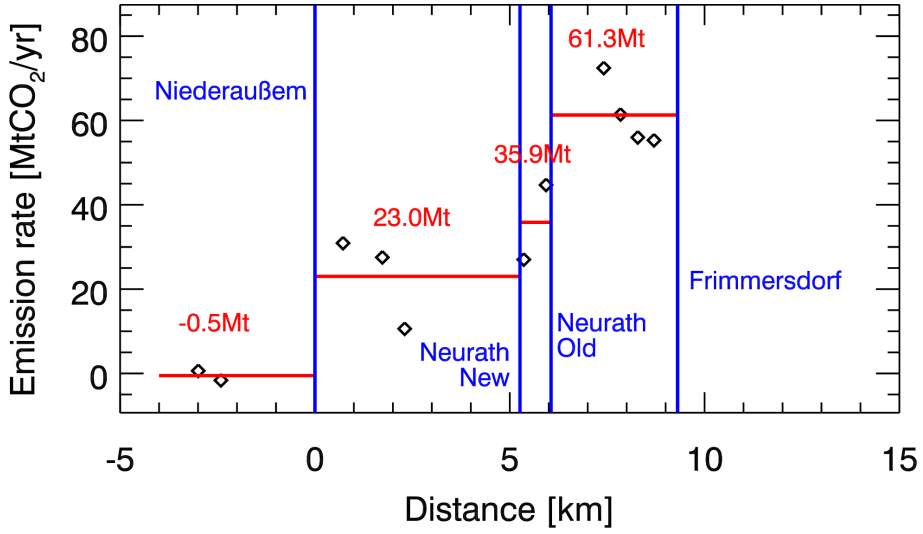

Figure 15. Mass balance results based on MAMAP remote sensing data. Vertical lines denote the location of power plants as downwind distance from Niederaußem. Horizontal lines and emission values show average total emissions of the upwind sources.

5.2.5 Error assessment

The influence of various parameters on the inversion results was investigated. This was mainly accomplished by evaluating errors introduced by uncertainties in the input parameters for the inversion methods, except for the statistical error on the plume inversion which yields about 3% for the total emission estimate and about 6% maximum error for a single power plant emission.

The computation of an average wind speed for the entire plume area (for the inverse plume model) and for the single tracks (when using the mass balance approach), respectively, is challenging. For this work the wind speed was estimated using a forward model for the plume dispersion assuming a single source at the location of Niederaußem power plant with an emission height of 250 m including initial plume rise. Furthermore a boundary layer depth of 1500 m was assumed. However, the boundary layer depth is not well defined (see Sect. 5.2.3) and the assumption of a single source is a simplification. To obtain a very rough estimate for the uncertainty on the resulting emission rates wind speeds were computed also for boundary layer depths of 1200 m and 1800 m, and similarly for emission heights of 200 m and 300 m.

For the mass balance approach the impact of the emission height on the emission results is less than 1% for the closest tracks and reduces for the transects further from the source. The error due to uncertainties in the boundary layer depth are largest for the far tracks since the plume will be more mixed. This results in an error of about -6% for the greater depth and an error of +4% for the reduced boundary layer depth.

For the inverse Gaussian plume model, the error on the emission height is always less than 0.5% and largest for the emission rate of Niederaußem. The impact of the boundary layer depth is very similar to that of the mass balance approach and within ±6%.

Atmos. Meas. Tech. Discuss., doi:10.5194/amt-2016-362, 2016
Manuscript under review for journal Atmos. Meas. Tech.
Published: 25 November 2016

Atmospheric Measurement Techniques Discussions

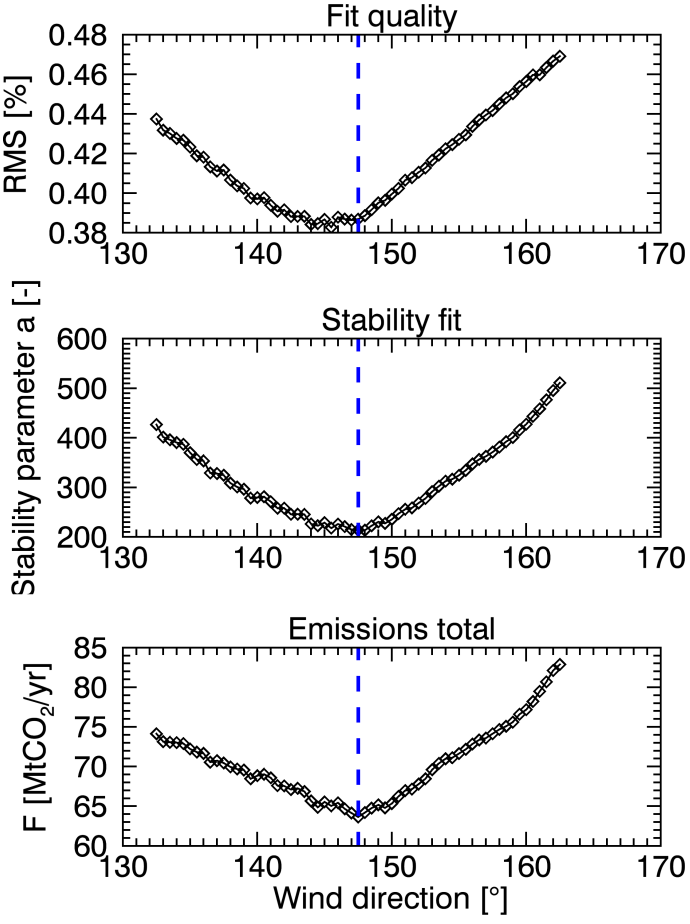

Figure 16. Sensitivity of the inverse Gaussian plume model to the wind direction.

These errors are similar to what can be assumed for the calibrated wind speed model of $\pm 0.5\,\mathrm{m\,s^{-1}}$ resulting in a percentage error of about $\pm 6\%$.

In cases where wind speed shows more pronounced variations with height, an average wind speed could be iteratively computed by weighting the sources according to the inversion result after using an a priori distribution of emissions for the initial state.

The wind direction of 147.5° for the inversion was determined by visually matching the best wind direction and minimizing the retrieved stability parameter a of the Gaussian plume inversion and hence minimizing the plume width relative to the centre axis (see Fig. 16). This also minimizes the total emission rate. However this minimum does not exactly coincide with the best fit (lowest RMS of differences between model and measurements) which is accomplished for about 145.5°. To account for the fact that the minimum in stability and fit quality is rather wide, an error of about ±4° was assumed. This results in errors on the emission rate of about $\pm 4\%$ for the mass balance approach and about $+6\%$ for total emissions from the inverse plume model.

Atmos. Meas. Tech. Discuss., doi:10.5194/amt-2016-362, 2016
Manuscript under review for journal Atmos. Meas. Tech.
Published: 25 November 2016

Atmospheric Measurement Techniques Discussions

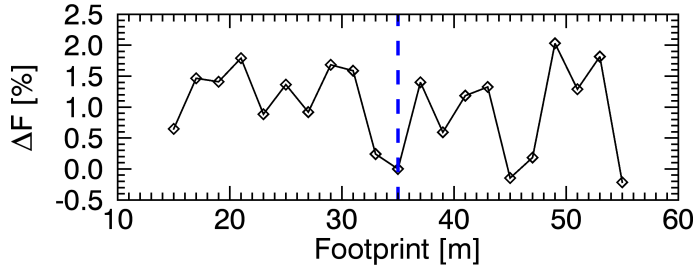

Figure 17. Sensitivity of the inverse Gaussian plume model result to the gridding size. The x-coordinate shows the edge length of a grid cell.

When varying the assumed source width by $\pm 200\,\mathrm{m}$ (baseline was $300\,\mathrm{m}$, for all power plants the same) the error for the inverse plume model is about $\mp 3\%$. The grid size was assumed to be $35\,\mathrm{m} \times 35\,\mathrm{m}$ which is not entirely correct since a MAMAP pixel for this work was rectangular (about $22.2\,\mathrm{m} \times 54.4\,\mathrm{m}$). The grid size was varied between $\pm 20\,\mathrm{m}$ resulting in errors of up to 2% but generally lower (see Fig. 17). Both error sources do not apply for the mass balance approach.

Several quality filters were applied to the data. The filter for fit quality RMS of 0.9% (see Fig. 6) has been set relatively broad to reject only the data of poorest quality. It does not improve the results to relax the filter further or apply a stricter criteria to reject data. The signal filter was set to reject data with a signal below 13000 counts (see Sect. 5.2.2). When relaxing the filter criteria by -2000 counts the total emission estimate is affected by about 6% for the plume inversion and about 1% for the mass balance approach. More strict filtering will significantly reduce the data which particularly impacts the mass balance and the defined plume area and was therefore not applied.

To avoid spurious results when the aircraft is turning (as the instruments optics was not mounted on a stabilization platform) an inclination filter was applied rejecting all data for inclination angles deviating more than 5° from the nadir geometry. Relaxing the filter to 10° results in changes for the total emission rate of about 5% for the inverse Gaussian plume and about 1% for the mass balance approach for the analyzed tracks furthest from the source.

The uncertainties derived above for the reasonable filter limits enter the final error budget.

Both inversion methods are impacted by the determination of the background CO_2 profile. For this work the profile was determined to $390\,\mathrm{ppm}$ (see Sect. 5.2.1). As in previous works (Krings et al., 2011, 2013) an uncertainty of approximately 1% was assumed leading to an uncertainty of 1% on the derived emission rates.

The error due to errors in the surface elevation model was not investigated. This is because they to a good extent cancel out for the proxy approach and high variations are not to be expected since the open cast mine relocation (compare Sect. 3) does not coincide with the measurement tracks of the remote sensing flight.

The overall errors (see Table 4) have been computed as root sum square assuming no correlation between errors and yielding about 10% for the mass balance and 15% for the plume inversion approach.

Atmos. Meas. Tech. Discuss., doi:10.5194/amt-2016-362, 2016
Manuscript under review for journal Atmos. Meas. Tech.
Published: 25 November 2016

Atmospheric Measurement Techniques Discussions

Table 4. Overview of maximum absolute values of the different error components of the estimated emission rates for the remote sensing results. The total error is the root sum square of the individual error components.

Error source	Mass balance approach	Inverse plume model
wind speed uncertainty	6%	6%
statistical error (maximum)	–	6%
emission height	1%	0.5%
boundary layer depth	6%	6%
wind direction	4%	6%
source width	–	3%
grid size	–	2%
signal filter	1%	6%
inclination filter	1%	5%
background profile	1%	1%
Total error	10%	15%

6 Discussion

The CO_2 emission rate estimates calculated using the different methods for the different power plants are shown in Fig. 18 and comprise the following: MAMAP remote sensing data analyzed with inverse plume model and mass balance approach, respectively, in-situ data analyzed using mass balance and emission rate estimates based on emission factors and energy production data for the time of the overflight. Error bars for the emissions derived from energy production are not shown. The error on power generation itself is generally about 1% (compare also Krings et al., 2011) and the annual error of derived emissions is required to be within 2.5% (European Commission, 2007). The error for the time of the overflight is most likely not much larger, although comparisons between U.S. inventories based on monitoring of stack gases with inventories based on emission factors can differ more than 20% for individual power plants (Ackerman and Sundquist, 2008).

Generally the two inversion approaches for MAMAP agree very well within their uncertainties for the three individual power plants.

When comparing with the CO_2 release computed from energy production the agreement is very good for all methods for the emissions from the power plant Niederaußem. For the two Neurath power plants, the remote sensing results indicate less emission from the new units and more from the old units while the overall result is approximately the same. This is then also reflected in the total emissions which are very similar for remote sensing methods and the computed emissions. The total emissions are 63.6, 61.3 und 63.8 $\mathrm{MtCO_2 yr^{-1}}$ for the MAMAP plume inversion, MAMAP mass balance and the computed emissions. The relative difference to the computed emissions is thereby -0.3% (plume inversion) and -3.9% (mass balance).

Atmos. Meas. Tech. Discuss., doi:10.5194/amt-2016-362, 2016
Manuscript under review for journal Atmos. Meas. Tech.
Published: 25 November 2016

Atmospheric Measurement Techniques Discussions

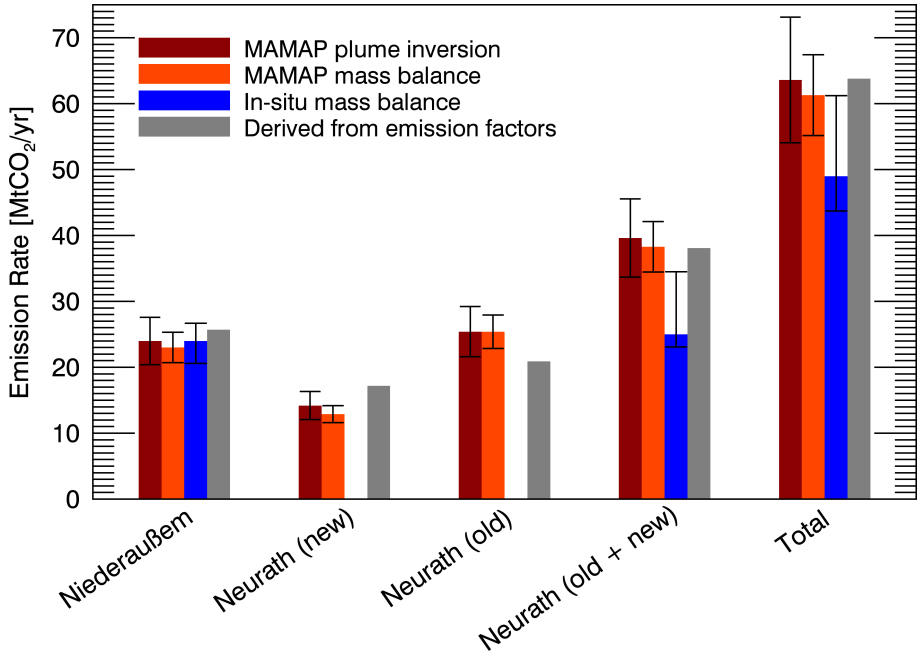

Figure 18. Inversion results compared to results obtained from emission factors and energy production for the time of the overflights. Error bars denote 1 σ errors for remote sensing, and the 10% and 90% percentile for in-situ (see Sect. 4.2.2).

If no in-situ data had been available, that is if the wind had been derived only from the COSMO-DE model, the errors would have been -6.4% and -10.0% respectively, reflecting the importance of additional wind measurements.

The total emissions derived from in-situ data are somewhat lower for the new and old blocks of power plant Neurath at 25.0 $\mathrm{MtCO_2 yr^{-1}}$ (23.1 to 34.5 $\mathrm{MtCO_2 yr^{-1}}$) and for the total at 49.0 $\mathrm{MtCO_2 yr^{-1}}$ (43.7 to 61.2 $\mathrm{MtCO_2 yr^{-1}}$). The reasons and uncertainties were explained in Sect. 5.1 and 4.2. However, the selection of the measurement day for detailed analysis was largely driven by the clear sky requirement for remote sensing and there was no ideal overlap between the optimal measurements from the in situ instruments and suitable remote sensing measurement days.

7 Conclusions

This work enhances the comparison between measurement and inversion approaches using in-situ and remote sensing data to obtain emission rates for flue gases from a cluster of point sources with known locations. These sources were partly in close proximity to each other and the plumes of – in this case – CO_2 from coal fired power plants overlapped adding complexity to the inverse problem.

In contrast to the in-situ method, the remote sensing measurements require clear sky conditions at the time of the measurement. This restriction impacted the selection of the measurement day for the analysis in this work. This resulted in some days with potentially more favorable conditions for the in-situ method (coverage, flight restrictions, etc.) being disregarded. Never-

Atmos. Meas. Tech. Discuss., doi:10.5194/amt-2016-362, 2016
Manuscript under review for journal Atmos. Meas. Tech.
Published: 25 November 2016

theless, the in-situ measurements for the selected day allowed a good estimate of the emission rate when the extrapolation to the upper limit of the mixed layer was applied (upper end of the error bar in Fig. 18).

Both remote sensing point source inversion methods are able to quantify the emissions within the error bars – 10% and 15% for the mass balance and plume inversion approach, respectively – assuming that the emissions derived from energy production which have been used for comparison are accurate within a few percent. The uncertainty for the mass balance result is lower because there are fewer input parameters that affect the overall result. It is, for example, not essential to know the exact source location and dimensions for the mass balance approach which is an advantage for surveying unknown sources with a non-imaging instrument like MAMAP. An imaging instrument with sufficient spatial resolution will be able to determine the source location from the data directly.

One critical external input parameter for the analysis of the remote sensing data is wind information, which in this work was derived using model and in-situ data. While the wind direction can be fitted to the data directly, this is not possible for the wind speed which scales linearly with the emission rate.

The in-situ inversion proves to be accurate for power plant Niederaußem where a complete sampling of the plume was possible. Further away from the sources, capturing the complete vertical plume extent in the higher reaching convective boundary layer was not possible due to airspace restrictions. Also the fact, that the background concentrations were derived from concentration minima in this widely contaminated area might have led to a negative bias for the estimated emissions.

While the individual results for remote sensing and in-situ yield very similar results provided sufficient sampling, a joint inversion approach may complement the individual methods also when there is no complete plume coverage.

The methods presented here are demonstrated for CO_2 emissions from point sources, however, they are directly applicable in the same way to other largely chemically inert gaseous compunds that disperse in the atmosphere such as, for example, CH_4 that is also derived from MAMAP remote sensing observations.

Appendix A: Wall alignment for the in-situ flux estimate

Discussing three possible problems assuming a misalignement of the wall (see Fig. 19), a widening of the plume within the wall, or a plume leaving the wall in another cell than it has entered. A_1 is the perfectly aligned wall element for the given wind vector v_w, with no cross wind component, where the plume crosses with a width of w_1. A_2 is misaligned by angle α with a cross wind component v_c, and A_3 is a wall element further downstream, where the plume might be wider (w_3). It is obvious from the graphics that $v_p = v_w \cos(\alpha)$, and $w_1 = w_2 \cos(\alpha)$, i.e. $w_2 = w_1 / \cos(\alpha)$. Since now $v_w \cdot w_1$ and $v_p \cdot w_2$ are equal, there is the same total mass transport across the wall (air or trace gas), even when the flux (mass per area and time) is reduced when misaligned. When the plume widens, the concentration is diluted accordingly, i.e. the total mass transport remains the same (also in two dimensions) as long as the flow (not the plume!) has no convergence or divergence within the wall. The interesting case is when a plume does not leave the wall in the same grid cell than it has entered it. In this case, both grid cells are associated with the same flux, i.e. the mass transport is doubled. This is also the case when a plume that is smaller than one grid cell is found in both cells (splitted). Conclusions: (i) the alignment with the mean wind should be adjusted because of

Atmos. Meas. Tech. Discuss., doi:10.5194/amt-2016-362, 2016
Manuscript under review for journal Atmos. Meas. Tech.
Published: 25 November 2016

Atmospheric Measurement Techniques Discussions

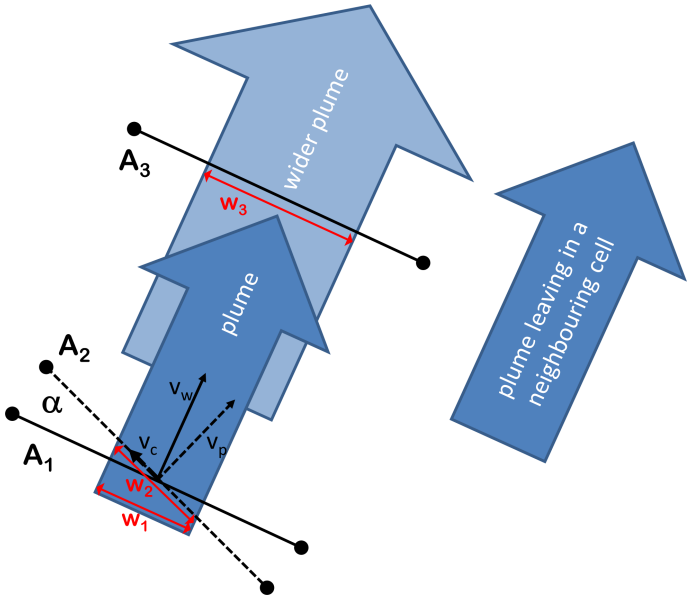

Figure 19. Figure illustrating misalignment of the wall for the in-situ flux estimate.

this third effect (this has absolute priority, i.e. the wall does not need to be aligned with the flight track, which was - in some cases - due to airspace restrictions - not crossing the plume perpendicularly); (ii) the size of the grid cells must not be too large to ensure correct determination of the background concentrations; (iii) as stated elsewhere, the variation of the grid size is a measure for the sensitivity.

Acknowledgements. The measurement campaign C-MAPExp was funded by the European Space Agency (ESA). The MAMAP activities are funded in parts by the University of Bremen and the State of Bremen. Wind data from the COSMO-DE model were obtained from the German Weather Service (DWD). The reference values for CO_2 emission rates of the power plants were derived from power generation values of each power plant location kindly provided by RWE AG, Essen, Germany. We acknowledge Armin Jordan from the Max Planck Institute for Biogeochemistry in Jena, Germany, for the analysis of airborne grab samples at the BGC GasLab.

Atmos. Meas. Tech. Discuss., doi:10.5194/amt-2016-362, 2016
Manuscript under review for journal Atmos. Meas. Tech.
Published: 25 November 2016

References

Ackerman, K. V. and Sundquist, E. T.: Comparison of Two U.S. Power-Plant Carbon Dioxide Emissions Data Sets, Environ. Sci. Technol., 42, 5688–5693, doi:10.1021/es800221q, 2008.

Allen, D. T., Torres, V. M., Thomas, J., Sullivan, D. W., Harrison, M., Hendler, A., Herndon, S. C., Kolb, C. E., Fraser, M. P., Hill, A. D., Lamb, B. K., Miskimins, J., Sawyer, R. F., and Seinfeld, J. H.: Measurements of methane emissions at natural gas production sites in the United States, Proceedings of the National Academy of Sciences, 110, 17 768–17 773, doi:10.1073/pnas.1304880110, http://www.pnas.org/content/110/44/17768.abstract, 2013.

Alvarez, R. A., Pacala, S. W., Winebrake, J. J., Chameides, W. L., and Hamburg, S. P.: Greater focus needed on methane leakage from natural gas infrastructure, Proceedings of the National Academy of Sciences, 109, 6435–6440, doi:10.1073/pnas.1202407109, http://www.pnas.org/content/109/17/6435.abstract, 2012.

Bovensmann, H., Buchwitz, M., Burrows, J. P., Reuter, M., Krings, T., Gerilowski, K., Schneising, O., Heymann, J., Tretner, A., and Erzinger, J.: A remote sensing technique for global monitoring of power plant CO_2 emissions from space and related applications, Atmos. Meas. Tech., 3, 781–811, doi:10.5194/amt-3-781-2010, 2010.

Bovensmann, H., Krings, T., Gerilowski, K., Neininger, B., Ruhtz, T., and Lindemann, C.: C-MAPExp Final Report - "Scientific and Technical Assistance for the Deployment of a flexible airborne spectrometer system during C-MAPExp", ESA Study, 2014.

Brandt, A. R., Heath, G. A., Kort, E. A., O'Sullivan, F., Pétron, G., Jordaan, S. M., Tans, P., Wilcox, J., Gopstein, A. M., Arent, D., Wofsy, S., Brown, N. J., Bradley, R., Stucky, G. D., Eardley, D., and Harriss, R.: Methane Leaks from North American Natural Gas Systems, Science, 343, 733–735, doi:10.1126/science.1247045, http://science.sciencemag.org/content/343/6172/733, 2014.

Buchwitz, M., Rozanov, V. V., and Burrows, J. P.: A near-infrared optimized DOAS method for the fast global retrieval of atmospheric CH_4, CO, CO_2, H_2O, and N_2O total column amounts from SCIAMACHY Envisat-1 nadir radiances, J. Geophys. Res., 105, 15 231–15 245, 2000.

Buchwitz, M., Reuter, M., Bovensmann, H., Pillai, D., Heymann, J., Schneising, O., Rozanov, V., Krings, T., Burrows, J. P., Boesch, H., Gerbig, C., Meijer, Y., and Löscher, A.: Carbon Monitoring Satellite (CarbonSat): assessment of atmospheric CO_2 and CH_4 retrieval errors by error parameterization, Atmospheric Measurement Techniques, 6, 3477–3500, doi:10.5194/amt-6-3477-2013, http://www.atmos-meas-tech.net/6/3477/2013/, 2013.

Cathles, L. M., Brown, L., Taam, M., and Hunter, A.: A commentary on "The greenhouse-gas footprint of natural gas in shale formations" by R.W. Howarth, R. Santoro, and Anthony Ingraffea, Climatic Change, 113, 525–535, doi:10.1007/s10584-011-0333-0, 10.1007/s10584-011-0333-0, 2012.

Caulton, D. R., Shepson, P. B., Santoro, R. L., Sparks, J. P., Howarth, R. W., Ingraffea, A. R., Cambaliza, M. O. L., Sweeney, C., Karion, A., Davis, K. J., Stirm, B. H., Montzka, S. A., and Miller, B. R.: Toward a better understanding and quantification of methane emissions from shale gas development, Proceedings of the National Academy of Sciences, 111, 6237–6242, doi:10.1073/pnas.1316546111, http://www.pnas.org/content/111/17/6237.abstract, 2014.

Ciais, P., Crisp, D., van der Gron, H. D., Engelen, R., Janssens-Maenhout, G., Heimann, M., Rayner, P., and Scholze, M.: Towards a European Opterational Observing System to Monitor Fossil CO_2 emissions, Final Report from the expert group, European Comission, 2015.

Doms, G.: A Description of the Nonhydrostatic Regional COSMO-Model, Deutscher Wetterdienst, Technical Report (http://www.cosmo-model.org/), last access: February 2015, 2011.

European Commission: Decision 2007/589/EC, establishing guidelines for the monitoring and reporting of greenhouse gas emissions pursuant to Directive 2003/87/EC of the European Parliament and of the Council, Official Journal of the European Union, L 229, 1–85, 2007.

Foken, T., Aubinet, M., Finnigan, J. J., Leclerc, M. Y., Mauder, M., and Paw U, K. T.: Results Of A Panel Discussion About The Energy Balance Closure Correction For Trace Gases, Bull. Amer. Meteor. Soc., 92, ES13–ES18, doi:10.1175/2011BAMS3130.1, 2009.

Frankenberg, C., Thorpe, A. K., Thompson, D. R., Hulley, G., Kort, E. A., Vance, N., Borchardt, J., Krings, T., Gerilowski, K., Sweeney, C., Conley, S., Bue, B. D., Aubrey, A. D., Hook, S., and Green, R. O.: Airborne methane remote measurements reveal heavy-tail flux distribution in Four Corners region, Proceedings of the National Academy of Sciences, 113, 9734–9739, doi:10.1073/pnas.1605617113, http://www.pnas.org/content/113/35/9734.abstract, 2016.

Gerilowski, K., Tretner, A., Krings, T., Buchwitz, M., Bertagnolio, P. P., Belemezov, F., Erzinger, J., Burrows, J. P., and Bovensmann, H.: MAMAP – a new spectrometer system for column-averaged methane and carbon dioxide observations from aircraft: Instrument description and performance analysis, Atmos. Meas. Tech., 4, 215–243, doi:10.5194/amt-4-215-2011, 2011.

Hiller, R. V., Neininger, B., Brunner, D., Gerbig, C., Bretscher, D., Künzle, T., Buchmann, N., and Eugster, W.: Aircraft-based CH_4 flux estimates for validation of emissions from an agriculturally dominated area in Switzerland, J. Geophys. Res, 119, 4874–4887, doi:10.1002/2013JD020918, 2014.

Howarth, R. W., Santoro, R., and Ingraffea, A.: Venting and leaking of methane from shale gas development: response to Cathles et al., Climatic Change, 113, 537–549, doi:10.1007/s10584-012-0401-0, 10.1007/s10584-012-0401-0, 2012.

IPCC: IPCC Guidelines for National Greenhouse Gas Inventories. Prepared by the National Greenhouse Gas Inventories Programme, Eggleston H.S., Buendia L., Miwa K., Ngara T. and Tanabe K. (eds.), Published: IGES, Japan., Volume 2, 2006.

Karion, A., Sweeney, C., Pétron, G., Frost, G., Michael Hardesty, R., Kofler, J., Miller, B. R., Newberger, T., Wolter, S., Banta, R., Brewer, A., Dlugokencky, E., Lang, P., Montzka, S. A., Schnell, R., Tans, P., Trainer, M., Zamora, R., and Conley, S.: Methane emissions estimate from airborne measurements over a western United States natural gas field, Geophysical Research Letters, 40, 4393–4397, doi:10.1002/grl.50811, 10.1002/grl.50811, 2013.

Kirschke, S., Bousquet, P., Ciais, P., Saunois, M., Canadell, J. G., Dlugokencky, E. J., Bergamaschi, P., Bergmann, D., Blake, D. R., Bruhwiler, L., Cameron-Smith, P., Castaldi, S., Chevallier, F., Feng, L., Fraser, A., Heimann, M., Hodson, E. L., Houweling, S., Josse, B., Fraser, P. J., Krummel, P. B., Lamarque, J.-F., Langenfelds, R. L., Quéré, C. L., Naik, V., O'Doherty, S., Palmer, P. I., Pison, I., Plummer, D., Poulter, B., Prinn, R. G., Rigby, M., Ringeval, B., Santini, M., Schmidt, M., Shindell, D. T., Simpson, I. J., Spahni, R., Steele, L. P., Strode, S. A., Sudo, K., Szopaand, S., van der Werf, G. R., Voulgarakis, A., van Weele, M., Weiss, R. F., Williams, J. E., and Zeng, G.: Three decades of global methane sources and sinks, Nature Geoscience, 6, 813–823, doi:10.1038/ngeo1955, 2013.

Krings, T., Gerilowski, K., Buchwitz, M., Reuter, M., Tretner, A., Erzinger, J., Heinze, D., Pflüger, U., Burrows, J. P., and Bovensmann, H.: MAMAP – A new spectrometer system for column-averaged methane and carbon dioxide observations from aircraft: retrieval algorithm and first inversions for point source emission rates, Atmos. Meas. Tech., 4, 1735–1758, doi:10.5194/amt-4-1735-2011, 2011.

Krings, T., Gerilowski, K., Buchwitz, M., Hartmann, J., Sachs, T., Erzinger, J., Burrows, J. P., and Bovensmann, H.: Quantification of methane emission rates from coal mine ventilation shafts using airborne remote sensing data, Atmos. Meas. Tech., 6, 151–166, doi:10.5194/amt-6-151-2013, 2013.

Lavoie, T. N., Shepson, P. B., Cambaliza, M. O. L., Stirm, B. H., Karion, A., Sweeney, C., Yacovitch, T. I., Herndon, S. C., Lan, X., and Lyon, D.: Aircraft-Based Measurements of Point Source Methane Emissions in the Barnett Shale Basin, Environ. Sci. Technol., 49, 7904–7913, doi:10.1021/acs.est.5b00410, 2015.

Martin, D. O.: The Change of Concentration Standard Deviations with Distance, J. Air Poll. Control Assoc., 26, 145–147, doi:10.1080/00022470.1976.10470238, 1976.

Masters, G. M.: Introduction to Environmental Engineering and Science, Prentice-Hall, Inc., 2nd edn., 1998.

Mays, K. L., Shepson, P. B., Stirm, B. H., Karion, A., Sweeney, C., and Gurney, K. R.: Aircraft-Based Measurements of the Carbon Footprint of Indianapolis, Environ. Sci. Technol., 43, 7816–7823, doi:10.1021/es901326b, 2009.

NRC: National Research Council (NRC) – Committee on Methods for Estimating Greenhouse Gas Emissions, Verifying Greenhouse Gas Emissions: Methods to Support International Climate Agreements, ISBN 0-309-15212-7, available from http://www.nap.edu/catalog/12883.html, last access: March, 2016, 2010.

Reuter, M., Buchwitz, M., Schneising, O., Hase, F., Heymann, J., Guerlet, S., Cogan, A. J., Bovensmann, H., and Burrows, J. P.: A simple empirical model estimating atmospheric CO_2 background concentrations, Atmospheric Measurement Techniques, 5, 1349–1357, doi:10.5194/amt-5-1349-2012, http://www.atmos-meas-tech.net/5/1349/2012/, 2012.

Schneising, O., Burrows, J. P., Dickerson, R. R., Buchwitz, M., Reuter, M., and Bovensmann, H.: Remote sensing of fugitive methane emissions from oil and gas production in North American tight geologic formations, Earth's Future, 2, 548–558, doi:10.1002/2014EF000265, http://dx.doi.org/10.1002/2014EF000265, 2014EF000265, 2014.

Thompson, D. R., Leifer, I., Bovensmann, H., Eastwood, M., Fladeland, M., Frankenberg, C., Gerilowski, K., Green, R. O., Kratwurst, S., Krings, T., Luna, B., and Thorpe, A. K.: Real-time remote detection and measurement for airborne imaging spectroscopy: a case study with methane, Atmos. Meas. Tech., 8, 4383–4397, doi:10.5194/amt-8-4383-2015, 2015.

Thorpe, A. K., Frankenberg, C., and Roberts, D. A.: Retrieval techniques for airborne imaging of methane concentrations using high spatial and moderate spectral resolution: application to AVIRIS, Atmospheric Measurement Techniques, 7, 491–506, doi:10.5194/amt-7-491-2014, 2014.

Tratt, D. M., Buckland, K. N., Hall, J. L., Johnson, P. D., Keim, E. R., Leifer, I., Westberg, K., and Young, S. J.: Airborne visualization and quantification of discrete methane sources in the environment, Remote Sensing of Environment, 154, 74–88, doi:10.1016/j.rse.2014.08.011, 2014.

Turner, D. B.: Workbook of Atmospheric Dispersion Estimates, U.S. Department of Health, Education, and Welfare, 95 pp., 1970.

U.S. Committee on Extension to the Standard Atmosphere: U.S. Standard Atmosphere, 1976, National Oceanic and Atmospheric Administration, National Aeronautics and Space Administration, United States Air Force, Washington D.C., 241 pp., 1976.

U.S. Environmental Protection Agency: Inventory of U.S. greenhouse gas emissions and sinks: 1990–2012. [Available at http://www.epa.gov/climatechange/Downloads/ghgemissions/US-GHG-Inventory-2014-Main-Text.pdf and http://www.epa.gov/climatechange/Downloads/ghgemissions/US-GHG-Inventory-2014-Annexes.pdf.], 2014.